# A Variational Approach to the Design of Multivariable Discrete-time Super-twisting-like Algorithms

Félix Miranda-Villatoro

# A Variational Approach to the Design of Multivariable Discrete-time Super-twisting-like Algorithms

(Author's version)

Félix A. Miranda-Villatoro
felix.miranda-villatoro@inria.fr
TRIPOP team at Centre Inria de l'Université Grenoble Alpes,
Grenoble INP, Laboratoire Jean Kuntzmann (LJK),
3800, Grenoble, France

**Abstract**

A family of discrete-time, super-twisting-like algorithms is presented. The algorithms are naturally vector-valued and are described in an implicit fashion, reminiscent of backward-Euler discretization schemes. The well-posedness of the closed-loop is established and the robust stability, against a family of external disturbances, is thoroughly studied. Implementation strategies, involving splitting-algorithms from convex optimization, are also discussed and compared. Finally, numerical simulations show the performance of the proposed schemes.

**Keywords:** Convex optimization, Discrete-time systems, Proximal-point algorithms, Robustness, Sliding-mode control, Splitting algorithms.

## 1 Introduction

The super-twisting algorithm (STA) [26] is one of the most popular schemes for control and observation in the family of high-order sliding mode methods. It has been vastly studied from a theoretical viewpoint (see *e.g.*, [15, 23, 27, 33, 36], and references therein), with recent extensions to stochastic systems [37] and infinite dimensional systems [4]. It is also used in a variety of engineering applications such as: control of mechanical systems [11], blood glucose regulation [22], trajectory tracking on quadrotor systems [12], reconstruction of atomic forces in probe microscopes [44], and control of wind energy conversion systems [14], to name just a few. Such success is due to its simple form, its robustness against external disturbances, and its intrinsic ability of diminishing the so called *chattering effect* in implementation. This reduction on chattering is mainly due to the fact that the control law is designed to be continuous, opposite to conventional first-order sliding controllers, where discontinuous signals drive the system's input directly [40, 41].

Nowadays, due to the versatility and the processing power of digital computers, it is common to carry out the control action in a discrete fashion. The resulting closed-loop, a discrete-time controller in feedback interconnection with a continuous-time plant, gives rise to an hybrid system [17, 28]. For this class of dynamical systems, guaranteeing the stability of closed-loop trajectories becomes a challenging task. A common partial solution relies on the *emulation* of the closed-loop in continuous time. That is, the controller is designed in continuous-time, so that the closed-loop meets all performance specifications. Afterwards, the resulting control strategy is discretized using an specific scheme, (such as backward-Euler, forward-Euler, mid-point rule, exact discretization, *etc.*) together with a sufficiently small sampling time, for approaching the continuous-time behavior. It is well-known that emulation may work for linear systems [16], specially when the backward-Euler scheme is used. However, that is not necessarily the case for non-smooth systems. Indeed, for the case of super-twisting controllers, emulation does not always yields a good performance when disturbances are in place. It has been shown in [3] that, the backward-Euler discretization of the super-twisting algorithm reported in [7], does not preserve the stability properties of the closed-loop, for any sampling time, when unbounded disturbances with bounded derivative are considered, whereas the continuous-time design does. This last fact motivates our departure from emulation, and leads us towards the context where the controller is conceived initially in

a discrete-time setting, by considering either: a robust analysis on a suitable time-sampled model of the plant (such as exact discretization) or an hybrid approach. Here we focus on the former scheme.

Several discrete-time versions of the super-twisting algorithm have been recently proposed, [3, 7, 19, 23, 38, 43]. All of them dealing with the scalar case and in most cases only asymptotic convergence is ensured. Also experimental results on emulation based super-twisting differentiations, using the backward-Euler discretization, can be found in [32]. In this work, a family of vector-valued discrete-time super-twisting-like algorithms is proposed. An important feature of the proposed algorithm is that it is grounded on the property of maximal monotonicity of the maps involved, and no homogeneity property is used. Indeed, maximal monotonicity allows us to make use of tools from convex optimization for both, the stability analysis of the closed-loop and the numerical implementation of the control law. The STA was originally formulated in continuous-time, for the scalar case, and its analysis was first done via geometric arguments [26]. Recently, some multivariable continuous-time extensions have been proposed, see *e.g.*, [5, 30, 34, 35, 42], dealing mainly with a component-wise extension of the scalar case and the so called unitary control approach [40]. In this work, the generalization to the multivariable case appears naturally, as all of the proofs and algorithms apply directly to the case of multiple controllers. This generality covers the control strategies already reported in the literature and paves the path towards new approaches.

The paper is organized as follows. After presenting preliminary material and the notation used along the manuscript in the next subsection, the closed-loop setup and the proposed family of discrete-time super-twisting-like algorithms under study are presented in Section 2. Next, the well-posedness of the closed-loop is studied in Section 3 and the stability properties of the origin are thoroughly analyzed in Section 4. Afterwards, a splitting strategy for the computation of the controller values, inspired by the Douglas-Rachford algorithm, is studied in Section 6. Finally, the paper ends with some conclusions in Section 7.

**Preliminaries and notations.**

The inner product in $\mathbb{R}^n$ is denoted as $\langle \cdot, \cdot \rangle$ and the $p$-norm of $w \in \mathbb{R}^n$ as $\|w\|_p = (\sum_{i=1}^n |w_i|^p)^{\frac{1}{p}}$. The set $\mathcal{B}$ denotes the open unit ball in $\mathbb{R}^n$. For any two sets $A, B \subset \mathbb{R}^n$, the set $A+B := \{a+b | a \in A, b \in B\}$. The notation $\mathrm{int}(A)$ denotes the interior of the set $A$, $\mathrm{cl}(A)$ its closure, and $\mathrm{rint}(A)$ its relative interior (*i.e.*, the interior of $A$ relative to its affine hull). Let $\mathbf{M} : \mathbb{R}^n \rightrightarrows \mathbb{R}^n$ be a set-valued map[1], the domain of $\mathbf{M}$ and the graph of $\mathbf{M}$ are the sets $\mathrm{Dom}\,\mathbf{M} := \{v \in \mathbb{R}^n \,|\, \mathbf{M}(v) \neq \emptyset\}$ and $\mathrm{Gph}\,\mathbf{M} := \{(v, w) \in \mathbb{R}^n \times \mathbb{R}^n \,|\, w \in \mathbf{M}(v)\}$, respectively. A set-valued map $\mathbf{M}$ is *monotone* if for any two pairs $(v_i, w_i) \in \mathrm{Gph}\,\mathbf{M}$, $i \in \{1, 2\}$,

$$0 \leq \langle v_1 - v_2, w_1 - w_2 \rangle . \tag{1}$$

It is strictly monotone if (1) holds with strict inequality for all $v_1 \neq v_2$. Further, $\mathbf{M}$ is called *maximal monotone*, if it is monotone and its graph is not strictly contained inside the graph of any other monotone operator. In addition, $\mathbf{M}$ is called $\theta$-monotone if there exists a continuous function $\theta : \mathbb{R}^n \times \mathbb{R}^n \to \mathbb{R}$ such that $\theta(x, y) = \theta(y, x)$ and for any two different pairs $(v_i, w_i) \in \mathrm{Gph}\,\mathbf{M}$, $i \in \{1, 2\}$,

$$\theta(v_1, v_2) \|v_1 - v_2\|_2 \leq \langle v_1 - v_2, w_1 - w_2 \rangle . \tag{2}$$

Maximal $\theta$-monotone operators are defined in an analogous way. It is clear that if $\theta \equiv 0$ in (2), then the map is monotone, whereas if $\theta(x, y) = \alpha \|x - y\|_2$, then $\mathbf{M}$ is strongly monotone (resp. hypomonotone) if $\alpha > 0$ (resp. $\alpha < 0$), the reader is addressed to [25] for further details on $\theta$-monotone maps.

A set-valued map $\mathbf{M}$ is *outer semicontinuous* at $v_0 \in \mathrm{Dom}\,\mathbf{M}$, if for any sequence $(v_n, w_n) \in \mathrm{Gph}\,\mathbf{M}$ such that $v_n \to v$ and $w_n \to w$ then $(v, w) \in \mathrm{Gph}\,\mathbf{M}$. It is well known that, in finite dimensions, maximal monotone operators are outer semicontinuous [8, Proposition 4.2.1-ii)].

Let $\Gamma_0(\mathbb{R}^n)$ denote the set of all convex, proper, lower-semicontinuous functions from $\mathbb{R}^n$ to $\mathbb{R} \cup \{+\infty\}$. For a function $f \in \Gamma_0(\mathbb{R}^n)$, the convex subdifferential $\partial f$ at a point $v \in \mathrm{Dom}\, f$, is defined as the set-valued map

$$\partial f(v) = \{w \in \mathbb{R}^n \,|\langle w, s - v \rangle \leq f(s) - f(v), \text{ for all } s \in \mathbb{R}^n\} . \tag{3}$$

It is well known that the subdifferential of a function $f \in \Gamma_0(\mathbb{R}^n)$ is maximal monotone, and therefore, also outer semicontinuous at all points of its domain.

The *proximal map* to the function $f \in \Gamma_0(\mathbb{R}^n)$ at $x$ is the map $\mathrm{Prox} : \mathbb{R}^n \to \mathbb{R}^n$ satisfying

$$\mathrm{Prox}_f(w) = \underset{s \in \mathbb{R}^n}{\arg\min} \left\{ f(s) + \frac{1}{2} \|s - w\|^2 \right\} .$$

[1] In this context set-valued means non-necessarily single-valued. Thus, single-valued functions are special cases of set-valued maps mapping points to singletons.

It follows that for any $w \in \mathbb{R}^n$, see *e.g.*, [6, Proposition 16.34],

$$\mathrm{Prox}_f(w) = (\mathrm{Id} + \partial f)^{-1}(w)\,, \tag{4}$$

where $\mathrm{Id} : \mathbb{R}^n \to \mathbb{R}^n$ denotes the identity map $x \mapsto x$. That is, $p = \mathrm{Prox}_f(w)$ is the unique solution to the *generalized equation*

$$0 \in p - w + \partial f(p)\,.$$

Moreover, Prox is a non-expansive map, *i.e.*, it is Lipschitz continuous with constant equal 1, (indeed, it is *firmly non-expansive* [6]).

The following lemma will be useful when studying the stability properties of the closed-loop.

**Lemma 1.** *Let $f \in \Gamma_0(\mathbb{R}^n)$ be such that $r\mathcal{B} \subset \partial f(0)$ for some $r > 0$. Then, for any $w \in \partial f(v)$ we have that $\|w\|_2 \geq r$ whenever $v \neq 0$.* ⌟

*Proof.* Let $(v, w) \in \mathrm{Gph}\,\partial f$ be arbitrary. By assumption, $(0, w') \in \mathrm{Gph}\,\partial f$ for any $w' \in r\mathcal{B}$, so that monotonicity of $\partial f$ implies that

$$\langle v, w\rangle \geq \sup_{w' \in r\mathcal{B}} \langle v, w'\rangle = r\,\|v\|_2\,.$$

The conclusion follows from the Cauchy-Schwarz inequality. □

## 2 Set-valued super-twisting-like controller

Consider the following $n$-dimensional perturbed integrator

$$\dot{x}(t) = u(t) + d(t)\,, \tag{5}$$

where $x(t), u(t), d(t) \in \mathbb{R}^n$, $d : \mathbb{R}_{\geq 0} \to \mathbb{R}^n$ is an unknown function accounting for time-dependent disturbances. The model (5) is general enough for the control of dynamical systems with relative degree 1 via sliding-mode control techniques, as it typically appears as the canonical dynamics of the sliding variable, see *e.g.*, [40] and Section 5 below. In what follows, $d$ is assumed independent of $x$ with an uniformly bounded time-derivative almost everywhere so that

$$\|\dot{d}(t)\| \leq M\,. \tag{6}$$

The main target consists in driving the state of (5) to the origin in finite time and in the presence of the disturbance $d$. To achieve that, we take inspiration from the following continuous-time super-twisting-like controller

$$u(t) \in -\gamma_1 K \partial f_1(x(t)) + \nu(t)\,, \tag{7a}$$
$$\dot{\nu}(t) \in -\gamma_2 K \partial f_2(x(t))\,, \tag{7b}$$

where the matrix $K \in \mathbb{R}^{n\times n}$ is symmetric positive definite, for each $i \in \{1, 2\}$, $\gamma_i > 0$ is a constant gain and each function $f_i \in \Gamma_0(\mathbb{R}^n)$, so that each $\partial f_i$ is a set-valued maximal monotone map. In the special case when $n = 1$, $f_1(\cdot) = \frac{2}{3}|\cdot|^{3/2}$, and $f_2(\cdot) = |\cdot|$, we retrieve the conventional super-twisting scheme. Note also that the controller (7) generalizes the conventional super-twisting algorithm in two directions. First, it is intrinsically multivariable. Second, it allows for general families of subdifferential maps $\partial f_i$, $i \in \{1, 2\}$, which may be either, single-valued or set-valued. This generalization departs from previous propositions [5, 30, 34, 35, 42], by identifying the maximal monotonicity of each subdifferential as the central property for studying the stability of the closed-loop, allowing to use powerful numerical schemes for the efficient numerical implementation, analysis, and design of the proposed super-twisting-like algorithm in a digital computer.

The following standing assumption is considered along the manuscript.

**Assumption 2.** $\mathrm{rint}(\mathrm{Dom}\, f_1) \cap \mathrm{rint}(\mathrm{Dom}\, f_2) \neq \emptyset$. ⌟

Assumption 2 guarantees that for any $K = K^\intercal \succ 0$, $\partial(f_1 + f_2) \circ K^{\frac{1}{2}}) = \partial(f_1 \circ K^{\frac{1}{2}}) + \partial(f_2 \circ K^{\frac{1}{2}})$ and $K^{\frac{1}{2}} \circ \partial f_i \circ K^{\frac{1}{2}} = \partial(f_i \circ K^{\frac{1}{2}})$, $i \in \{1, 2\}$, see Theorem 16.37 in [6]. Assumption 2 is used below to guarantee the well-posedness of the proposed discrete-time model, as it is shown in the next section.

Throughout this paper we consider the case in which the control law (7) is designed in a discrete-time framework, having in mind that its implementation can be realized via a digital computer, whereas the

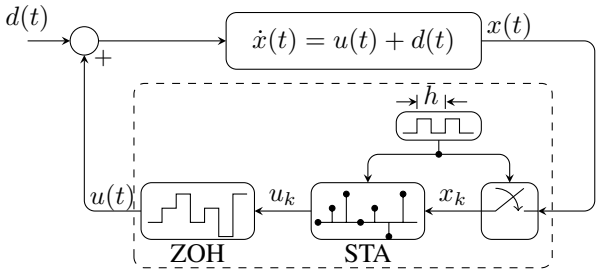


Figure 1: Closed-loop setup. The state of the continuous-time plant is sampled at regular intervals of length $h$. Such information is used to compute the control law at discrete-time intervals, and this last one is applied to the continuous-time plant via a zero-order-hold (ZOH) mechanism.

state of the continuous-time plant (5) is sampled at constant time intervals of length $h := t_{k+1} - t_k > 0$. Figure 1 below depicts the resulting closed-loop.

Taking into account that the control signal $u(t)$ is piecewise constant, the following discrete-time model describes the dynamics of the perturbed plant at the sampling times $\{t_k\}_{k\in\mathbb{N}}$,

$$x_{k+1} = x_k + hu_k + h\bar{d}_k\,, \tag{8a}$$
$$\bar{d}_{k+1} = \bar{d}_k + h\Delta_k\,, \tag{8b}$$

where the "averaged perturbation" $\bar{d}_k = \frac{1}{h}\int_{t_k}^{t_{k+h}} d(\tau)d\tau$ is unknown and $\Delta_k$ is uniformly bounded. The second equation comes from the use of the mean-value theorem for definite integrals at each component of the vector $d(t)$. Namely, component-wise we have that, for some $\tau_k^{(i)} \in [t_k, t_k + h]$

$$\bar{d}_{i,k} = \frac{1}{h}\int_{t_k}^{t_k+h} d_i(\tau)d\tau = d_i(\tau_k^{(i)})\,.$$

Hence, there exist $\tau_k^{(i)} \in [t_k, t_k + h]$ and $\tau_{k+1}^{(i)} \in [t_k + h, t_k + 2h]$ such that the following holds,

$$\bar{d}_{i,k+1} - \bar{d}_{i,k} = d_i(\tau_{k+1}^{(i)}) - d_i(\tau_k^{(i)}) = \tilde{h}_k^{(i)}\dot{d}_i(\theta_k^{(i)})\,,$$

for some $\theta_k^{(i)} \in [\tau_k^{(i)}, \tau_{k+1}^{(i)}]$, where $\tilde{h}_k^{(i)} := \tau_{k+1}^{(i)} - \tau_k^{(i)}$. Setting $\Delta_{i,k} = \frac{\tilde{h}_k^{(i)}}{h}\dot{d}_{i,k}$ leads us to (8b) and it follows from (6) that $\|\Delta_k\|_2 \leq 2M$.

Regarding the discrete-time controller, it has the following form

$$u_k = -K(\gamma_1 m_{1,k} + h\gamma_2 m_{2,k}) + \nu_{k+1} \tag{9a}$$
$$\nu_{k+1} = \nu_k - h\gamma_2 K m_{2,k} \tag{9b}$$
$$m_{i,k} \in \partial f_i(\varrho(x_k, u_k)), \quad i \in \{1, 2\}, \tag{9c}$$

where $K = K^\intercal \succ 0$, $\gamma_i > 0$ and each $f_i \in \Gamma_0(\mathbb{R}^n)$ satisfies Assumption 2 for $i \in \{1, 2\}$. Finally, $\varrho : \mathbb{R}^n \times \mathbb{R}^n \to \mathbb{R}^n$ is a known function that depends on the state $x_k$ and the control $u_k$, whose explicit form is specified below. Thus, the controller (9) above is defined in an *implicit* fashion, as it takes the form

$$u_k \in \nu_{k+1} - K\partial(\gamma_1 f_1 + h\gamma_2 f_2)(\tilde{x}_{k+1})\,, \tag{10a}$$
$$\nu_{k+1} \in \nu_k - h\gamma_2 K\partial f_2(\tilde{x}_{k+1})\,, \tag{10b}$$
$$\tilde{x}_{k+1} = \varrho(x_k, u_k)\,. \tag{10c}$$

The introduction of the dummy variable $\tilde{x}_{k+1}$ was proposed for the first time in [2] in the context of backward-Euler emulation of sliding controllers. In there, such variable has the interpretation of *nominal* state, as in the absence of disturbances, $\tilde{x}_{k+1} = x_{k+1}$, and it plays a fundamental role for the numerical implementation of the controller. In this work we go a step further and use $\tilde{x}_{k+1}$ as a variable to be designed, so that it reaches the origin in finite time and the state $x_k$ shows robustness against matched disturbances. In particular, we are not restricted by the equality $\tilde{x}_{k+1} = x_{k+1}$ when disturbances are absent.

Conditions establishing the well-posedness (existence and uniqueness of solutions) of the closed-loop (8)-(9) are presented in the following section. The main differences between the discrete-time controller

(9) (equivalently, (10)) and those already reported in the state-of-the-art literature, (as for instance [7], [23] and [3]), consists on the choice of the map $\varrho$ used here and the addition of the term $-h\gamma_2 K m_{2,k}$ in (9a). Indeed, it is shown below that these differences allow us to establish the finite-time stability of the origin for the multivariable nominal case (notice that in [3] and [23], only asymptotic stability is proved, whereas [7] deals with the backward-Euler emulation of the conventional super-twisting algorithm in the scalar case), as well as, to improve the robustness of the closed-loop when unbounded disturbances (with bounded derivative) are considered.

In what follows it is shown that the closed-loop (8)-(9) is well-posed in a multivariable context and with general functions $f_i \in \Gamma_0(R^n)$ satisfying Assumption 2. The main property that allows us to extend the design to more general cases than those reported in [7], [3], is the maximal monotonicity of the subdifferentials in (9c). Such property turns out to be also central for the efficient computation of the control signals, as is shown in Section 6 below.

## 3 Well-posedness of the closed-loop

In this section the well-posedness (existence and uniqueness of solutions) of the scheme (8)-(9) is studied. We start by defining the function $\varrho$ as

$$\varrho(x_k, u_k) = x_k + hu_k - h\nu_{k+1}\,, \tag{11}$$

so that the closed-loop system becomes

$$x_{k+1} = \tilde{x}_{k+1} + h(\nu_{k+1} + \bar{d}_k) \tag{12a}$$
$$\bar{d}_{k+1} = \bar{d}_k + h\Delta_k \tag{12b}$$
$$\nu_{k+1} = \nu_k - h\gamma_2 K m_{2,k} \tag{12c}$$
$$\tilde{x}_{k+1} = x_k - hK(\gamma_1 m_{1,k} + h\gamma_2 m_{2,k}) \tag{12d}$$
$$m_{i,k} \in \partial f_i(\tilde{x}_{k+1}),\ i \in \{1,2\} \tag{12e}$$

It is worth to remark that the function $\varrho$ in (11) differs from the one proposed in [7]. Indeed, in [7] the function considered is $\varrho_b(x_k, u_k) = x_k + hu_k$. Such choice is the result of the emulation of the continuous-time closed-loop system (5)-(7) using the backward-Euler discretization. It is shown in [3] that the resulting controller is not robust with respect to unbounded disturbances with bounded derivative. In contrast, (11) does not shows such an issue. Thus, preserving one characteristic feature of the continuous-time super-twisting algorithm.

Now, taking the change of coordinates $z_{1,k} = K^{-\frac{1}{2}} x_k$, $z_{2,k} = K^{-\frac{1}{2}}(\nu_k + \bar{d}_{k-1})$, (recalling that $K = K^\intercal \succ 0$, it follows that the proposed change of coordinates is well-defined), the closed-loop system (8)-(9) becomes

$$z_{1,k+1} = \tilde{z}_{1,k+1} + hz_{2,k+1} \tag{13a}$$
$$z_{2,k+1} = z_{2,k} - h\gamma_2 \hat{m}_{2,k} + h\hat{\Delta}_{k-1} \tag{13b}$$
$$\tilde{z}_{1,k+1} = z_{1,k} - h\gamma_1 \hat{m}_{1,k} - h^2\gamma_2 \hat{m}_{2,k} \tag{13c}$$
$$\hat{m}_{i,k} \in \partial \hat{f}_i(\tilde{z}_{1,k+1}),\ i \in \{1,2\} \tag{13d}$$

where $\hat{m}_{i,k} = K^{\frac{1}{2}} m_{i,k}$, $\hat{\Delta}_k = K^{-\frac{1}{2}}\Delta_k$, $\hat{f}_i = f_i \circ K^{\frac{1}{2}} \in \Gamma_0(\mathbb{R}^n)$, for $i \in \{1,2\}$. Notice that Assumption 2 was used for obtaining (13d). It is clear that the well-posedness of (13) is equivalent to that of (12).

The following theorem ensures that with the above assumptions the closed-loop (13) is well-posed. That is, for any initial condition $z_{1,0}, z_{2,0} \in \mathbb{R}^n$ there exist unique sequences $\{z_{1,k}\}_{k\in\mathbb{N}}$, $\{z_{2,k}\}_{k\in\mathbb{N}}$, $\{\hat{m}_{1,k}\}_{k\in\mathbb{N}}$ and $\{\hat{m}_{2,k}\}_{k\in\mathbb{N}}$ satisfying (13) for all $k \in \mathbb{N}$. In addition, the selections $\hat{m}_{1,k} \in \partial \hat{f}_1(\tilde{z}_{1,k+1})$ and $\hat{m}_{2,k} \in \partial \hat{f}_2(\tilde{z}_{1,k+1})$ depend only on data and system parameters available at time $t_k = kh$.

**Theorem 3.** *Let $f_i \in \Gamma_0(\mathbb{R}^n)$, for $i \in \{1,2\}$, such that Assumption 2 holds. In addition, let $D_i$ be the set of points where $\hat{f}_i$ is non-differentiable. If $D_1 \cap D_2 = \emptyset$, then for any initial condition $(z_{1,0}, z_{2,0}) \in \mathbb{R}^n \times \mathbb{R}^n$, (13) has a unique solution.* ⌟

*Proof.* Let $g = \gamma_1 \hat{f}_1 + h\gamma_2 \hat{f}_2 \in \Gamma_0(\mathbb{R}^n)$, it follows from (13c) and (13d) that

$$z_{1,k} \in (\mathrm{Id} + h\partial g)(\tilde{z}_{1,k+1})\,. \tag{14}$$

Hence, in view of (4), $\tilde{z}_{1,k+1}$ is given by

$$\tilde{z}_{1,k+1} = \mathrm{Prox}_{hg}(z_{1,k})\,. \tag{15}$$

Since $\mathrm{Prox}_{hg}$ is a single-valued Lipschitz continuous function, then $\tilde{z}_{1,k+1}$ is uniquely determined by the function $g$, the time-step $h$, and the value of the state $z_{1,k}$, all of them available at time $t_k = kh$. Now, the substitution of (15) back into (13c) yields

$$\gamma_1 \hat{m}_{1,k} + h\gamma_2 \hat{m}_{2,k} = \frac{1}{h}\left(\mathrm{Id} - \mathrm{Prox}_{hg}\right)(z_{1,k})\,. \tag{16}$$

Hence, the sum $\gamma_1 \hat{m}_{1,k} + h\gamma_2 \hat{m}_{2,k}$ is also uniquely determined by the function $g$ and the state $z_{1,k}$. However, note that (16) alone does not guarantee the uniqueness of each selection $\hat{m}_{i,k}$, $i \in \{1,2\}$ in (13d). Now, if $D_1 \cap D_2 = \emptyset$, then for any $\tilde{z}_{1,k+1}$ either: $\partial \hat{f}_1(\tilde{z}_{1,k+1}) = \{\nabla \hat{f}_1(\tilde{z}_{k+1})\}$ or $\partial \hat{f}_2(\tilde{z}_{1,k+1}) = \{\nabla \hat{f}_2(\tilde{z}_{k+1})\}$. In the former case $\hat{m}_{1,k}$ is uniquely determined by (13d) and $\hat{m}_{2,k}$ is the unique point in $\partial \hat{f}_2(\tilde{z}_{1,k+1})$ satisfying (16), whereas in the latter case, $\hat{m}_{2,k}$ is uniquely determined by (13d) and $\hat{m}_{1,k}$ is the unique point in $\partial \hat{f}_1(\tilde{z}_{1,k+1})$ satisfying (16). Thus, in any case the values of $\hat{m}_{1,k}$ and $\hat{m}_{2,k}$ are uniquely determined by (13d), (16), the state $z_{1,k}$, and known parameters. Finally, it is clear from (13b) that $z_{2,k+1}$ depends only of terms available at time $t_k$ and the external disturbance $\hat{\Delta}_{k-1}$ so that the closed-loop (13) admits a unique solution. □

The well-posedness of the original system (12) follows directly from Theorem 3. Notice that in (13) the state $z_{2,k}$ is unavailable for feedback, as it depends on the disturbance $\hat{\Delta}_{k-1}$. Nevertheless, the control strategy $u_k$ in (10)-(11) is implementable, since it depends on $z_{1,k} = K^{-\frac{1}{2}} x_{1,k}$, $\nu_k$ and known parameters.

For conventional multivariable super-twisting algorithms, such as those proposed in [30, 35], the maps $f_1(\cdot) = \frac{2}{3}\|\cdot\|_2^{\frac{3}{2}}$ and $f_2(\cdot) = \|\cdot\|_2$ with $K = I_m$ are used, such that $\hat{f}_i = f_i$ for $i \in \{1,2\}$. With such choice, Theorem 3 guarantees the well-posedness of the closed-loop as $f_1$ is continuously differentiable, so that $D_1 = \emptyset$. The following proposition illustrates the explicit form of the control strategy.

**Proposition 4** (Unitary super-twisting algorithm)**.** *The explicit form of the selection values $m_{i,k}$ in* (12e) *with $K = \kappa I_n \succ 0$, $f_1(\cdot) = \phi_1(\cdot) + \frac{\alpha_1}{2}\|\cdot\|_2^2$, $f_2(\cdot) = \phi_2(\cdot) + \frac{\alpha_2}{2}\|\cdot\|_2^2$, where $\phi_1(\cdot) = \frac{2}{3}\|\cdot\|_2^{\frac{3}{2}}$, $\phi_2(\cdot) = \|\cdot\|_2$, and $\alpha_i \geq 0$, $i \in \{1,2\}$ is given by*

$$m_{1,k} = \begin{cases} 0, & \text{if } \frac{\|x_k\|_2}{h^2\gamma_2\kappa} \leq 1\,; \\ \dfrac{\left(\kappa^{\frac{1}{4}} + \alpha_1 \kappa^{\frac{1}{2}} q(\kappa^{-\frac{1}{2}} x_k)\right) q(\kappa^{-\frac{1}{2}} x_k)}{\|x_k\|_2} x_k, & \text{otherwise.} \end{cases} \tag{17a}$$

$$m_{2,k} = \begin{cases} \dfrac{1}{h^2\gamma_2\kappa^{\frac{1}{2}}} x_k, & \text{if } \frac{\|x_k\|_2}{h^2\gamma_2\kappa} \leq 1\,; \\ \dfrac{1 + \alpha_2 \kappa^{\frac{1}{2}} q\left(\kappa^{-\frac{1}{2}} x_k\right)^2}{\|x_k\|_2} x_k, & \text{otherwise.} \end{cases} \tag{17b}$$

*where $q : \mathbb{R}_+ \setminus h^2\gamma_2\kappa^{\frac{1}{2}}\mathcal{B} \to \mathbb{R}_+$ is such that*

$$q(v) = -\frac{h\gamma_1\kappa^{\frac{3}{4}}}{2\beta} + \frac{1}{2\beta}\sqrt{h^2\gamma_1^2\kappa^{\frac{3}{2}} + 4\beta(v - h^2\gamma_2\kappa^{\frac{1}{2}})} \tag{18}$$

*and $\beta = 1 + h\kappa(\alpha_1\gamma_1 + h\alpha_2\gamma_2)$.* ⌟

*Proof.* We start by considering the closed-loop (13) and later we apply the corresponding transformation to get the original control selections. It is easy to verify that the associated functions $\hat{f}_i = f_i \circ K^{\frac{1}{2}}$, $i \in \{1,2\}$, satisfy all the hypothesis stated in Theorem 3. The closed-loop (13) is rewritten equivalently as

$$z_{1,k+1} = \tilde{z}_{1,k+1} + h z_{2,k+1} \tag{19a}$$

$$z_{2,k+1} = z_{2,k} - h\kappa\gamma_2\alpha_2 \tilde{z}_{1,k+1} - h\gamma_2 \hat{\mu}_{2,k} + h\hat{\Delta}_{k-1} \tag{19b}$$

$$\tilde{z}_{1,k+1} = \frac{1}{\beta} z_{1,k} - \frac{h}{\beta}(\gamma_1 \hat{\mu}_{1,k} + h\gamma_2 \hat{\mu}_{2,k}) \tag{19c}$$

$$\hat{\mu}_{i,k} \in \partial\hat{\phi}_i(\tilde{z}_{1,k+1}),\ i \in \{1,2\} \tag{19d}$$

where $\hat{\phi}_j = \phi_j \circ K^{\frac{1}{2}}$, $j \in \{1,2\}$, so that

$$\hat{m}_{i,k} = \hat{\mu}_{i,k} + \alpha_i \kappa \tilde{z}_{1,k+1} \in \partial \hat{f}_i(\tilde{z}_{1,k+1}), \quad i \in \{1,2\}\,. \tag{20}$$

It is noteworthy that, with the new structure (19), the computations of both, $\tilde{z}_{1,k+1}$ and the control values $\hat{m}_{i,k}$, $i \in \{1,2\}$, are simplified. Concretely, setting $\Phi := \gamma_1\hat{\phi}_1 + h\gamma_2\hat{\phi}_2$ it follows from (19c)-(19d) (and the definition of proximal map), that

$$\tilde{z}_{1,k+1} = \mathrm{Prox}_{\frac{h}{\beta}\Phi}\left(\frac{1}{\beta}z_{1,k}\right), \tag{21}$$

$$\gamma_1\hat{\mu}_{1,k} + h\gamma_2\hat{\mu}_{2,k} = \frac{\beta}{h}\left(\mathrm{Id} - \mathrm{Prox}_{\frac{h}{\beta}\Phi}\right)\left(\frac{1}{\beta}z_{1,k}\right), \tag{22}$$

Since $\hat{\phi}_1$ is continuously differentiable, then $\partial\hat{\phi}_1$ is single-valued and

$$\hat{\mu}_{1,k} = \nabla\hat{\phi}_1 \circ \mathrm{Prox}_{\frac{h}{\beta}\Phi}\left(\frac{1}{\beta}z_{1,k}\right) \tag{23a}$$

$$h\gamma_2\hat{\mu}_{2,k} = \frac{\beta}{h}\left(\mathrm{Id} - \mathrm{Prox}_{\frac{h}{\beta}\Phi}\right)\left(\frac{1}{\beta}z_{1,k}\right) - \gamma_1\nabla\hat{\phi}_1 \circ \mathrm{Prox}_{\frac{h}{\beta}\Phi}\left(\frac{1}{\beta}z_{1,k}\right) \tag{23b}$$

It remains to obtain an explicit expression for the proximal map $\mathrm{Prox}_{\frac{h}{\beta}\Phi} = (\mathrm{Id} + \frac{h}{\beta}\partial\Phi)^{-1}$ at the point $\frac{1}{\beta}z_{1,k}$. To that end, we proceed as follows. First notice that $\tilde{z}_{1,k+1} = \mathrm{Prox}_{\frac{h}{\beta}\Phi}(\frac{1}{\beta}z_{1,k})$ if, and only if, $\tilde{z}_{1,k+1}$ is the solution to the following generalized equation

$$\frac{1}{\beta}z_{1,k} \in \tilde{z}_{1,k+1} + \frac{h}{\beta}\left(\gamma_1\kappa^{\frac{3}{4}}\|\tilde{z}_{1,k+1}\|_2^{\frac{1}{2}} + h\gamma_2\kappa^{\frac{1}{2}}\right)\partial\|\tilde{z}_{1,k+1}\|_2\,. \tag{24}$$

where,

$$\partial\|y\|_2 = \begin{cases} \frac{1}{\|y\|_2}y, & \text{if } y \neq 0 \\ \mathrm{cl}(\mathcal{B}), & \text{otherwise} \end{cases}. \tag{25}$$

From (24) it is clear that $\tilde{z}_{1,k+1} = 0$, if and only if, $z_{1,k} \in h^2\gamma_2\kappa^{\frac{1}{2}}\,\mathrm{cl}(\mathcal{B})$. Indeed, if $\tilde{z}_{1,k+1} = 0$, then clearly (24)-(25) imply that $z_{1,k} \in h^2\gamma_2\kappa^{\frac{1}{2}}\,\mathrm{cl}(\mathcal{B})$. On the contrary, if $\tilde{z}_{1,k+1} \neq 0$, then $z_{1,k}$ and $\tilde{z}_{1,k+1}$ are collinear, since the substitution of (25) into (24) yields

$$\frac{z_{1,k}}{\beta} = \left(1 + \frac{h(\gamma_1\kappa^{\frac{3}{4}}\|\tilde{z}_{1,k+1}\|_2^{\frac{1}{2}} + h\gamma_2\kappa^{\frac{1}{2}})}{\beta\,\|\tilde{z}_{1,k+1}\|_2}\right)\tilde{z}_{1,k+1}\,, \tag{26}$$

so that, the 2-norm of $z_{1,k}$ satisfies

$$\|z_{1,k}\|_2 = \beta\|\tilde{z}_{1,k+1}\|_2 + h\gamma_1\kappa^{\frac{3}{4}}\|\tilde{z}_{1,k+1}\|_2^{\frac{1}{2}} + h^2\gamma_2\kappa^{\frac{1}{2}}\,, \tag{27}$$

so that $z_{1,k} \notin h^2\gamma_2\kappa^{\frac{1}{2}}\,\mathrm{cl}(\mathcal{B})$ and the conclusion follows. Moreover, solving (27) with respect to $\|\tilde{z}_{1,k+1}\|_2^{\frac{1}{2}}$, leads us to

$$0 \leq \|\tilde{z}_{1,k+1}\|_2^{\frac{1}{2}} = q(\|z_{1,k}\|_2)\,, \tag{28}$$

with $q(\|z_{1,k}\|_2)$ as in (18). Hence, it follows from (26)-(28) that for $z_{1,k} \notin h^2\gamma_2\kappa^{\frac{1}{2}}\,\mathrm{cl}(\mathcal{B})$,

$$\tilde{z}_{1,k+1} = \left(1 + \frac{h\left(\gamma_1\kappa^{\frac{3}{4}}q(z_{1,k}) + h\gamma_2\kappa^{\frac{1}{2}}\right)}{\beta q(z_{1,k})^2}\right)^{-1}\frac{z_{1,k}}{\beta} = \frac{q(z_{1,k})^2}{\|z_{1,k}\|_2}z_{1,k}\,. \tag{29}$$

Putting all together, the explicit expression for $\tilde{z}_{1,k+1}$ is obtained as

$$\tilde{z}_{1,k+1} = \mathrm{Prox}_{\frac{h}{\beta}\Phi}\left(\frac{z_{1,k}}{\beta}\right) = \begin{cases} 0, & \text{if } \|z_{1,k}\|_2 \leq h^2\gamma_2\kappa^{\frac{1}{2}}\,; \\ \frac{q(z_{1,k})^2}{\|z_{1,k}\|_2}z_{1,k}, & \text{otherwise.} \end{cases} \tag{30}$$

Therefore, from (23), $\hat{\mu}_{1,k}$ and $\hat{\mu}_{2,k}$ are given by

$$\hat{\mu}_{1,k} = \nabla\hat{\phi}_1(\tilde{z}_{1,k+1}) = \begin{cases} 0, & \text{if } \|z_{1,k}\|_2 \leq h^2\gamma_2\kappa^{\frac{1}{2}}\,; \\ \kappa^{\frac{3}{4}}\frac{q(z_{1,k})}{\|z_{1,k}\|_2}z_{1,k}, & \text{otherwise.} \end{cases} \tag{31a}$$

$$\hat{\mu}_{2,k} = \frac{\beta}{h^2\gamma_2}(\mathrm{Id} - \mathrm{Prox}_{\frac{h}{\beta}\Phi})\left(\frac{z_{1,k}}{\beta}\right) - \frac{\gamma_1}{h\gamma_2}\hat{\mu}_{1,k} = \begin{cases} \frac{1}{h^2\gamma_2}z_{1,k}, & \text{if } \|z_{1,k}\|_2 \leq h^2\gamma_2\kappa^{\frac{1}{2}}\,; \\ \frac{\kappa^{\frac{1}{2}}}{\|z_{1,k}\|_2}z_{1,k}, & \text{otherwise}\,. \end{cases} \tag{31b}$$

Finally, we retrieve the expressions in (17) after using (20) and recalling that $m_{i,k} = \kappa^{-\frac{1}{2}}\hat{m}_{i,k}$ and $x_k = \kappa^{\frac{1}{2}}z_{1,k}$. □

It is noteworthy that, for the particular case when $n = 1$, $\kappa = 1$, and $\alpha_1 = \alpha_2 = 0$, then the closed-loop (12) reduces to the one studied in [3, Section III].

## 4 Stability properties of the set-valued super-twisting-like controller

In this section we study the stability properties of the closed-loop (13). To that end, let us consider the following standing assumption.

**Assumption 5.** *The function $\hat{f}_2 \in \Gamma_0(\mathbb{R}^n)$ has a unique minimizer at the origin, so that $0 \in \operatorname{int}(\partial \hat{f}_2(0))$.*

Assumption 5 excludes maps $\hat{f}_2$ that are continuously differentiable around zero, as it stipulates that $\partial \hat{f}_2(0)$ is neither the empty set nor a singleton.

**Proposition 6.** *Let Assumption 5 and all the assumptions of Theorem 3 hold. If for some $k^* \in \mathbb{N}$, $z_{1,k^*-1}, z_{1,k^*} \in h\partial g(0)$, where $g = \gamma_1 \hat{f}_1 + h\gamma_2 \hat{f}_2$, then $\tilde{z}_{1,k^*+r} = 0$ for all $r \in \mathbb{N}$, whenever $0 < \gamma_1$ and $0 < \gamma_2$ is such that $\hat{\Delta}_k \in \gamma_2 \partial \hat{f}_2(0)$ for all $k \in \mathbb{N}$.* ⌟

*Proof.* It follows from (14) that if both, $z_{1,k^*-1}, z_{1,k^*} \in h\partial g(0)$, then $\tilde{z}_{1,k^*} = \tilde{z}_{1,k^*+1} = 0$. Consequently, (13a) and (13c) lead us to

$$z_{2,k^*} = \gamma_1 \hat{m}_{1,k^*} + h\gamma_2 \hat{m}_{2,k^*} \,,$$

and from (13a)-(13b) it follows that

$$z_{1,k^*+1} \in h\gamma_1 \partial \hat{f}_1(0) + h^2 \gamma_2 \partial \hat{f}_2(0) \,. \tag{32}$$

Therefore, $\tilde{z}_{1,k^*+2} = 0$ and the conclusion follows by using an induction argument. This concludes the proof. □

Proposition 6 shows that in the cases when $\operatorname{int}(\partial g(0)) \neq \emptyset$, the invariance of $\{z \in \mathbb{R}^{2n} \,|\tilde{z}_{1,k} = 0\}$ is robust against the presence of disturbances $\hat{\Delta}_k$. Following [20] we say that the closed-loop (13) is in *discrete-time sliding-mode* whenever $\tilde{z}_{1,k} = 0$ for all $k \geq k^*$. It is shown next that, during such stage, the control input becomes insensitive to increments on the value of the gains (Corollary 8).

We now turn our attention towards the study of stability of the origin of the closed-loop (13). Let us introduce the virtual variable $\tilde{z}_{2,k+1} = z_{2,k} - h\gamma_2 \hat{m}_{2,k}$, so that the closed-loop (13) is rewritten as:

$$z_{1,k+1} = \tilde{z}_{1,k+1} + h\tilde{z}_{2,k+1} + h^2 \hat{\Delta}_{k-1} \tag{33a}$$
$$z_{2,k+1} = \tilde{z}_{2,k+1} + h\hat{\Delta}_{k-1} \tag{33b}$$
$$\tilde{z}_{1,k+1} = z_{1,k} - h\gamma_1 \hat{m}_{1,k} - h^2 \gamma_2 \hat{m}_{2,k} \tag{33c}$$
$$\tilde{z}_{2,k+1} = z_{2,k} - h\gamma_2 \hat{m}_{2,k} \tag{33d}$$
$$\hat{m}_{i,k} \in \partial \hat{f}_i(\tilde{z}_{1,k+1}) \tag{33e}$$

Notice that the subsystem (33c)-(33e) does not depend directly on disturbance terms and it is well-defined by Theorem 3. The following theorem shows that the proposed super-twisting-like algorithm drives the virtual variables $\tilde{z}_{i,k+1}$, $i \in \{1, 2\}$, towards zero in finite time, whereas the original variables rest ultimately bounded in neighborhoods of the origin whose size is proportional to the time-step and the upper-bound on the disturbance.

**Theorem 7.** *Consider the closed-loop (33). Let Assumption 5 and all the assumptions of Theorem 3 hold. Let $\hat{f}_1$ be continuous differentiable around zero, so that $0 = \nabla \hat{f}_1(0)$ and $\nabla \hat{f}_1$ is maximal $\theta$-monotone with $\theta(v_1, v_2) > 0$ for all $v_1 \neq v_2 \in \mathbb{R}^n$ and $\theta(v, v) = 0$. Hence, if $\|\hat{\Delta}_k\| \leq \eta$ for all $k \in \mathbb{N}$ and some $\eta \geq 0$, then there exist sufficiently large gains $\gamma_1 > 0$, $\gamma_2 > \eta$, and a finite $k^* \in \mathbb{N}$, such that $\tilde{z}_{1,k+1} = 0$ and $\tilde{z}_{2,k+1} = 0$ for all $k \geq k^*$. In particular, $z_{1,k+1}$ and $z_{2,k+1}$ are ultimately bounded and satisfy $z_{1,k+1} \in h^2 \eta \operatorname{cl}(\mathcal{B})$ and $z_{2,k+1} \in h\eta \operatorname{cl}(\mathcal{B})$ for all $k \geq k^*$.* ⌟

*Proof.* From (33) it follows that

$$\tilde{z}_{1,k+1} = \tilde{z}_{1,k} + h\tilde{z}_{2,k+1} - h\gamma_1 \hat{m}_{1,k} \,, \tag{34a}$$
$$\tilde{z}_{2,k+1} = \tilde{z}_{2,k} - h\gamma_2 \hat{m}_{2,k} + h\hat{\Delta}_{k-2} \,. \tag{34b}$$

Let us consider the following positive definite function

$$V_{k+1} = \gamma_2(\hat{f}_2(\tilde{z}_{1,k+1}) - \hat{f}_2(0)) + \frac{1}{2}\left\|\tilde{z}_{2,k+1} - \gamma_1\hat{m}_{1,k}\right\|_2^2 . \tag{35}$$

Notice that $V_{k+1} = 0$ if and only if $\tilde{z}_{1,k+1} = \tilde{z}_{2,k+1} = 0$. It follows from the definition of subdifferential in (3) and (34) that the mismatch $V_{k+1} - V_k$ satisfies

$$V_{k+1} - V_k \leq -\frac{1}{2}\left\|\tilde{z}_{2,k+1} - \gamma_1\hat{m}_{1,k} - (\tilde{z}_{2,k} - \gamma_1\hat{m}_{1,k-1})\right\|_2^2 - \frac{\gamma_1}{h}\langle\hat{m}_{1,k} - \hat{m}_{1,k-1}, \tilde{z}_{1,k+1} - \tilde{z}_{1,k}\rangle + h\langle\hat{\Delta}_{k-2}, \tilde{z}_{2,k+1} - \gamma_1\hat{m}_{1,k}\rangle . \tag{36}$$

Recalling that by assumption $\partial\hat{f}_1$ is $\theta$-strongly monotone, it follows that

$$V_{k+1} - V_k \leq -\frac{1}{2}\left\|\tilde{z}_{2,k+1} - \gamma_1\hat{m}_{1,k} - (\tilde{z}_{2,k} - \gamma_1\hat{m}_{1,k-1})\right\|_2^2 - \frac{\gamma_1}{h}\theta(\tilde{z}_{1,k+1}, \tilde{z}_{1,k})\left\|\tilde{z}_{1,k+1} - \tilde{z}_{1,k}\right\|_2$$
$$+h\left\|\hat{\Delta}_{k-2}\right\|_2\left\|\tilde{z}_{2,k+1} - \gamma_1\hat{m}_{1,k}\right\|_2 = -\frac{1}{2}\left\|\tilde{z}_{2,k+1} - \gamma_1\hat{m}_{1,k} - (\tilde{z}_{2,k} - \gamma_1\hat{m}_{1,k-1})\right\|_2^2 - (\gamma_1\theta(\tilde{z}_{1,k+1}, \tilde{z}_{1,k}) - h\eta)\left\|\tilde{z}_{2,k+1} - \gamma_1\hat{m}_{1,k}\right\|$$

Thus, $V_{k+1} - V_k \leq 0$ whenever $\theta(\tilde{z}_{1,k+1}, \tilde{z}_{1,k}) \geq \frac{h}{\gamma_1}\eta$. In what follows it is shown that indeed the origin of subsystem (34) is finite-time stable. To that end, it follows from (37) and classical arguments (see *e.g.*, [24, Corollary 4.8.6 and 4.11.2]), that for $\gamma_1$ sufficiently large, there exists $k^* \in \mathbb{N}$ for which

$$\left\|\tilde{z}_{2,k+1} - \gamma_1\hat{m}_{1,k}\right\|_2 \leq h\delta_1(\gamma_1) \text{ for all } k \geq k^* . \tag{38}$$

Hence, from (34a) $\left\|\tilde{z}_{1,k+1} - \tilde{z}_{1,k}\right\|_2 \leq h^2\delta_1(\gamma_1)$ and as $\partial\hat{f}_1 = \nabla\hat{f}_1$ is continuous with $0 = \nabla\hat{f}_1(0)$, it follows that there exists $\varepsilon_1(\gamma_1)$ such that

$$\left\|\hat{m}_{1,k} - \hat{m}_{1,k-1}\right\| \leq h\varepsilon_1(\gamma_1) \text{ for all } k \geq k^* . \tag{39}$$

Note that, as $\gamma_1$ gets larger, both, $\varepsilon_1(\gamma_1)$ and $\delta_1(\gamma_1)$, can be chosen smaller. Now, by combining (38)-(39) it is inferred that

$$\left\|\tilde{z}_{2,k+1} - \tilde{z}_{2,k}\right\|_2 \leq h(2\delta_1(\gamma_1) + \gamma_1\varepsilon_1(\gamma_1)) \text{ for all } k \geq k^* + 1 . \tag{40}$$

Therefore, from (34b) we obtain the following upper bound for the term $\hat{m}_{2,k}$

$$\left\|\hat{m}_{2,k}\right\|_2 \leq \frac{2\delta_1(\gamma_1) + \gamma_1\varepsilon_1(\gamma_1) + \eta}{\gamma_2} . \tag{41}$$

Note that, for $\gamma_1$ and $\gamma_2$ sufficiently large, $\left\|\hat{m}_{2,k}\right\|_2 \leq r$ for all $k \geq k^* + 1$ and some $r > 0$ such that $r\mathcal{B} \subset \partial\hat{f}_2(0)$. Since $\hat{m}_{2,k} \in \partial\hat{f}_2(\tilde{z}_{1,k+1})$, it follows from Lemma 1 that $\tilde{z}_{1,k+1} = 0$ for all $k \geq k^* + 1$. Moreover, since $\nabla\hat{f}_1(0) = 0$, then $\hat{m}_{1,k} = 0$. Hence, (34) implies that $\tilde{z}_{2,k+1} = 0$ for all $k \geq k^* + 1$, and finite-time stability of the zero solution of (34) follows. Finally, the bounds on $z_{1,k+1}$ and $z_{2,k+1}$ follow directly from (33a)-(33b). This concludes the proof. □

It is noteworthy that the proposed discrete-time algorithm (9) achieves a precision of order $\mathcal{O}(h^2)$ in $z_{1,k+1}$, which is the variable of interest. This is consistent with the order of the continuous-time super-twisting algorithm, which is 2. In contrast, the precision achieved by the scalar backward-Euler emulation in [7] is of order $\mathcal{O}(h)$. Clearly, in the absence of disturbances, the origin of (33) (equiv. (12) and (13)) is globally finite-time stable. Also, notice that the ultimate bounds on $z_{1,k+1}$ and $z_{2,k+1}$ are independent of the gains $\gamma_1$ and $\gamma_2$ and depend only on the sampling time $h$ and the bound on the disturbance term $\hat{\Delta}_k$. The following corollary brings some light into such independence property.

**Corollary 8.** *Let all assumptions of Theorem 7 hold. There is $k^* < \infty$ such that $\tilde{z}_{1,k+1} = \tilde{z}_{2,k+1} = 0$ and $u_k = -\bar{d}_{k-1}$ for all $k > k^*$. That is, the control law* (9) *(and therefore the closed-loop* (12)*, equiv.* (13) *and* (33)*) is insensitive against increments on the values of the gains $\gamma_1$ and $\gamma_2$ once the sliding phase has been reached.* ⌟

*Proof.* The proof follows by noticing that $\tilde{z}_{1,k+1} = \tilde{z}_{2,k+1} = 0$ for all $k > k^*$, implies that *i)* $\hat{m}_{1,k} = 0$, and *ii)* $z_{2,k} = h\gamma_2\hat{m}_{2,k}$ for all $k > k^*$. Thereby, as $z_{2,k} = K^{-\frac{1}{2}}(\nu_{k+1} + \bar{d}_{k-1})$, it is inferred that $u_k = -K(\gamma_1 m_{1,k} + h\gamma_2 m_{2,k}) + \nu_{k+1} = \nu_{k+1} - h\gamma_2 K m_{2,k} = -\bar{d}_{k-1}$ for all $k > k^*$. Therefore, the controller is independent of the explicit value of the gains. □

Corollary 8 is akin to first-order set-valued sliding-mode controllers [20], [31], where the explicit values of the gain only affect the reaching phase. During the sliding phase, the precise value of the gain is irrelevant, just a minimum bound has to be respected to maintain the discrete-time sliding motion. In that case, any increment on the values of the gains will have no effect on the closed-loop, as the controller is *automatically* compensating for the disturbance with one-step delay. In other words, over-estimation of the control gains has no effect on the closed-loop once the sliding surface has been reached. To the best of author's knowledge, this property of gain invariance is unique to selection-based controllers. It was first shown theoretically in [20] and it has also been confirmed in experimental setups in [21], for the case of backward-Euler emulation of first-order sliding controllers. Such invariance represents an important advantage against implementations based on arbitrary graph approximations and *ad-hoc* regularizations of the non-smooth maps involved.

## 5 An attitude stabilization problem

Let us consider the problem of attitude stabilization of a fully actuated rigid body. The attitude of a rigid body, relative to a given reference frame, is represented uniquely by an orthonormal matrix $R \in SO(3) := \{R \in \mathbb{R}^{3\times 3} \,|\, \det(R) = 1, \text{ and } R^{-1} = R^\intercal\}$, see *e.g.*, [9], [18]. The kinematics of the rigid-body attitude is described by

$$\frac{d}{dt}R(t) = R(t)\omega(t)^\times, \tag{42}$$

where $\omega(t)$ denotes the angular velocity of the body, relative to a reference frame, $(\cdot)^\times$ denotes the conventional isomorphism between $\mathfrak{so}(3)$ (the tangent space to $SO(3)$ at $R = I$) and $\mathbb{R}^3$, that is

$$\omega^\times = \begin{bmatrix} 0 & -\omega_3 & \omega_2 \\ \omega_3 & 0 & -\omega_1 \\ -\omega_2 & \omega_1 & 0 \end{bmatrix}.$$

Assuming that the control action provides torques along the principal edges of the rigid body, the attitude dynamics is then expressed in the body's frame via Euler's equation

$$J\frac{d}{dt}\omega(t) = (J\omega(t))^\times\omega(t) + \tau(t) + d(t)\,, \tag{43}$$

where $J = J^\intercal \succ 0$ denotes the inertia matrix, $\tau(t) \in \mathbb{R}^3$ is the control action, and $d(t)$ denotes the external disturbances. Given an initial attitude $R_0 \in SO(3)$ and initial angular velocity $\omega_0 \in \mathbb{R}^3$, our objective consists in designing $\tau(t)$ so that the full state is regulated at $R_d = I \in SO(3)$, $\omega_d = 0$ regardless of the disturbance $d(t)$.

For designing the discrete-time controller, we consider the following discrete-time approximation to (42)-(43)

$$R_{k+1} = R_k\Gamma_k\,, \tag{44a}$$

$$J\omega_{k+1} = J\omega_k + h(J\omega_k)^\times\omega_k + h(\tau_k + d_k)\,, \tag{44b}$$

where $\Gamma_k = \left(I + \frac{h}{2}\omega_k^\times\right)\left(I - \frac{h}{2}\omega_k^\times\right)^{-1}$. The discrete model (44) is the result of a mid-point discretization in the attitude $R(t)$, together with a forward Euler discretization of $\omega(t)$ in (42)-(43). It is not difficult to see that the mid-point discretization with respect to $R$ ensures the positive invariance of $SO(3)$ with respect to (44a). To achieve the regulation task, we consider the sliding variable $\sigma_k$ proposed in [18] as

$$\sigma_k = \omega_k + \text{vex}(\mathbb{P}_\text{a}(R_k)), \tag{45}$$

where $\mathbb{P}_\text{a} : \mathbb{R}^{3\times 3} \to \mathfrak{so}(3)$ mapping $R \mapsto \frac{1}{2}(R - R^\intercal)$, and vex : $\mathfrak{so}(3) \to \mathbb{R}^3$ is the inverse map to $(\cdot)^\times$. It was proved in [18] that, for the continuous-time problem, $R = I$, $\omega = 0$ is an almost globally stable equilibrium of (42)-(43) on $\mathcal{D} := \{(R, \omega) \in SO(3) \times \mathbb{R}^3 \,|\sigma(R, \omega) = 0\}$. The same conclusion holds for the discrete-time case presented here. Indeed, whenever $\sigma_k = 0$, it follows from (45) that $\omega_k^\times = -\mathbb{P}_\text{a}(R_k)$ such that (44a) reduces to

$$R_{k+1} = R_k\left(I - \frac{h}{2}\,\mathbb{P}_\text{a}(R_k)\right)\left(I + \frac{h}{2}\,\mathbb{P}_\text{a}(R_k)\right)^{-1}. \tag{46}$$

Notice also that if $R_k = I$, then $\omega_k^\times = 0$ whenever $\sigma_k = 0$. Thus, to solve the regulation problem we need to ensure the finite-time stability of the origin in the sliding dynamics associated with (45) and the asymptotic stability of $R = I$ in (46). The following proposition shows that indeed, $R = I$ is almost globally stable for the reduced system (46).

**Proposition 9.** *$R = I$ is an almost globally asymptotically stable equilibrium of the reduced dynamics (46), whenever $h < 2s$.* ⌟

*Proof.* Let us consider the following Lyapunov function candidate, as proposed in [18]

$$V_{k+1} = \frac{1}{2}\operatorname{tr}(I - R_{k+1}). \tag{47}$$

Hence,

$$\begin{aligned} V_{k+1} - V_k &= -\frac{1}{2}\operatorname{tr}(R_{k+1} - R_k) \\ &= \frac{h}{2}\operatorname{tr}\left(R_k\,\mathbb{P}_{\mathrm{a}}(R_k)\left(I + \frac{h}{2}\,\mathbb{P}_{\mathrm{a}}(R_k)\right)^{-1}\right). \end{aligned} \tag{48}$$

Recalling that $R_k \in SO(3)$ for all $k \in \mathbb{N}$, it follows that the argument inside the trace of (48) is a matrix function of $R_k$, denoted as $\Phi$, so that

$$V_{k+1} - V_k = \frac{h}{2}\operatorname{tr}(\Phi(R_k)) = \frac{h}{2}\sum_{i=1}^{3}\phi(\lambda_{i,k}) \tag{49}$$

where $\lambda_{i,k} \in \operatorname{spect}(R_k)$, $\operatorname{spect}(R) \subset \mathbb{C}$ denotes the spectrum of $R$, and

$$\phi(\lambda) = \lambda\frac{\lambda - \frac{1}{\lambda}}{2}\left(1 + \frac{h}{4}\left(\lambda - \frac{1}{\lambda}\right)\right)^{-1} = \frac{2\lambda\,\mathrm{Im}(\lambda)(h\,\mathrm{Im}(\lambda) + \mathrm{j}2)}{4 + (h\,\mathrm{Im}(\lambda))^2}, \tag{50}$$

where we have used the fact that for a matrix $R \in SO(3)$, $\lambda - \frac{1}{\lambda} = \mathrm{j}2\,\mathrm{Im}(\lambda)$ for any $\lambda \in \operatorname{spect}(R)$. Indeed, the spectrum of $R_k \in SO(3)$ is given as

$$\operatorname{spect}(R_k) = \{1, \alpha_k + \mathrm{j}\beta_k, \alpha_k - \mathrm{j}\beta_k\},\ \text{s.t. } \alpha_k^2 + \beta_k^2 = 1. \tag{51}$$

Thus, It follows from (49)-(51) that

$$\begin{aligned} V_{k+1} - V_k &= \frac{2h\beta_k}{4 + (h\beta_k)^2}\,\mathrm{Re}\left((\alpha_k + \mathrm{j}\beta_{\mathrm{k}})(h\beta_k + \mathrm{j}2)\right) \\ &= -\frac{2h\beta_k^2(2 - h\alpha_k)}{4 + (h\beta_k)^2}. \end{aligned} \tag{52}$$

Since $0 \le \alpha_k \le 1$ for all $k \in \mathbb{N}$, $V_{k+1} - V_k \le 0$ for all $k \in \mathbb{N}$ so that $R = I$ is a stable equilibrium and convergence follows using the same arguments as in the proof of Theorem 2 in [18]. □

Now that the stability of the desired solution (of the reduced dynamics) has been established, we focus on the finite-time stability of the discrete sliding dynamics which is obtained from (44)-(45) as

$$\begin{aligned} J\sigma_{k+1} &= J\omega_{k+1} + J\operatorname{vex}(\mathbb{P}_{\mathrm{a}}(R_{k+1})) \\ &= J\sigma_k + h(J\omega_k)^{\times}\omega_k + h(\tau_k + d_k) + J\operatorname{vex}(\mathbb{P}_{\mathrm{a}}(R_{k+1} - R_k)). \end{aligned} \tag{53}$$

It follows from (44a) and the definition of $\Gamma_k$ that $R_{k+1} - R_k = \frac{h}{2}(R_{k+1} + R_k)\omega_k^{\times} = \frac{h}{2}R_k(\Gamma_k + I)\omega_k^{\times}$ so that the sliding dynamics results into

$$J\sigma_{k+1} = J\sigma_k + h(J\omega_k)^{\times}\omega_k + h(\tau_k + d_k) + \frac{h}{2}J\operatorname{vex}\left(\mathbb{P}_{\mathrm{a}}(R_k(\Gamma_k + I)\omega_k^{\times})\right). \tag{54}$$

Thus, setting

$$\tau_k = Ju_k - (J\omega_k)^{\times}\omega_k - \frac{1}{2}J\operatorname{vex}\left(\mathbb{P}_{\mathrm{a}}(R_k(\Gamma_k + I)\omega_k^{\times})\right), \tag{55}$$

leads us to the sliding dynamics

$$\sigma_{k+1} = \sigma_k + hu_k + hJ^{-1}d_k, \tag{56}$$

Clearly, (56) has the same form as (8). In order to drive $\sigma_k$ towards the origin in finite time, the super-twisting-like algorithm (9), as developed in Proposition 4, is considered with $x_k = \sigma_k$. Notice that for $\phi_1(v) = \frac{2}{3}\|v\|_2^{\frac{3}{2}}$, the subdifferential $\partial\phi_1$ is $\theta$-monotone with

$$\theta(v_a, v_b) = \frac{\|v_a - v_b\|_2}{\|v_a\|_2^{\frac{1}{2}} + \|v_b\|_2^{\frac{1}{2}}}.$$

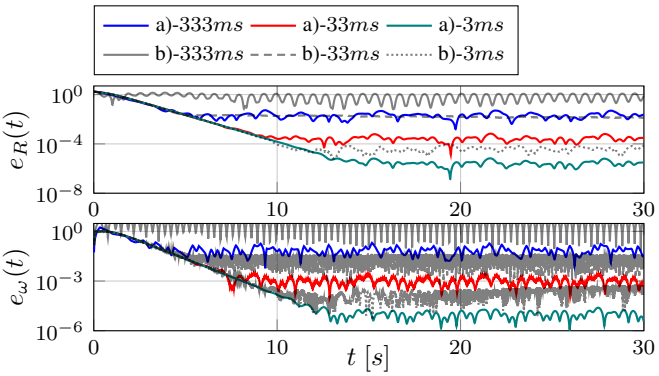


Figure 2: Time trajectories of the error norms $e_R(t) = \|I - R(t)\|_2$ and $e_\omega(t) = \|\omega(t)\|_2$ for three different sampling times ($333ms, 33ms$, and $3ms$). Case a) corresponds to trajectories with the feedback (9), (17), whereas case b) corresponds to trajectories with the feedback (58). In all cases the system is affected by the disturbance (57).

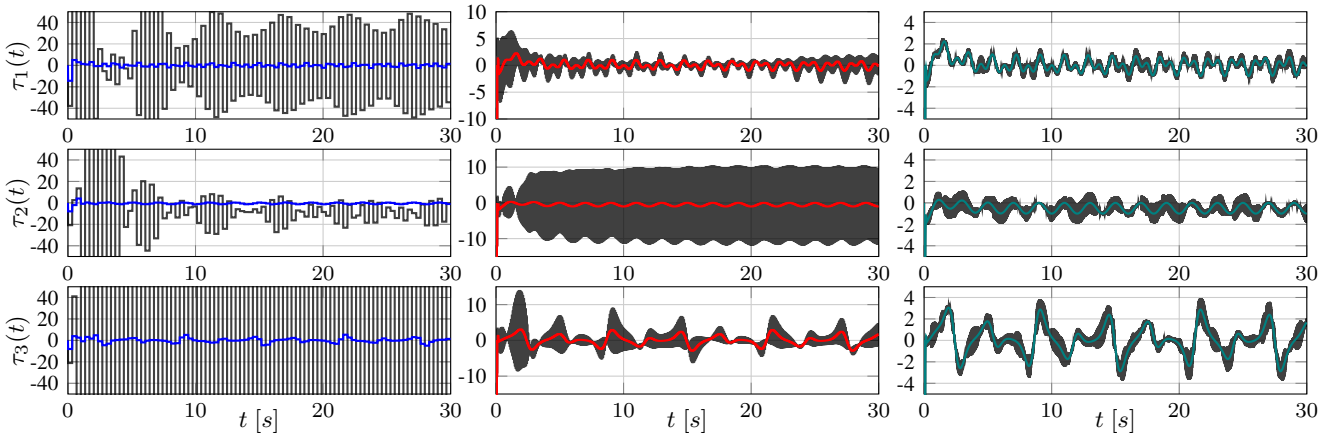


Figure 3: Time evolution of the control input $\tau(t) = \tau_k$ for $t \in [kh, (k+1)h)$ with $\tau_k$ as in (55) for three different sampling times ($333ms$ (left column), $33ms$ (central column) and $3ms$ (right column)). For each sampling time two cases are considered: *i)* $u_k$ as in (9), (17) (color lines) and *ii)* $u_k$ as in (58) (gray lines). It can be noted that, as the sampling frequency increases, both controllers become alike.

| | $\gamma_1 = 15, \gamma_2 = 30$ | | | $\gamma_1 = 0.1, \gamma_2 = 300$ | | | $\gamma_1 = 300, \gamma_2 = 24$ | | | $\gamma_1 = 300, \gamma_2 = 300$ | | |
|---|---|---|---|---|---|---|---|---|---|---|---|---|
| samp/sec | 3 | 30 | 300 | 3 | 30 | 300 | 3 | 30 | 300 | 3 | 30 | 300 |
| $\|u_a\|_{L^2}$ | 17.95 | 13.94 | 13.75 | 17.95 | 23.16 | 31.37 | 17.95 | 19.11 | 38.09 | 17.95 | 24.94 | 38.44 |
| $\|u_b\|_{L^2}$ | 971 | 57.56 | 14.92 | – | 102e6 | 1120 | – | 39e3 | 2553 | – | 38e3 | 2537 |
| $\|e_{R_a}\|_{L^\infty}$ | 50e−3 | 67e−5 | 67e−7 | 50e−3 | 67e−5 | 67e−7 | 50e−3 | 67e−5 | 67e−7 | 50e−3 | 67e−5 | 67e−7 |
| $\|e_{R_b}\|_{L^\infty}$ | 12e−1 | 17e−3 | 69e−6 | – | 19e−1 | 19e−1 | – | 10e−1 | 70e−5 | – | 16e−1 | 20e−4 |
| $\|e_{\omega_a}\|_{L^\infty}$ | 18e−2 | 25e−4 | 25e−6 | 18e−2 | 25e−4 | 25e−6 | 18e−2 | 25e−4 | 25e−6 | 18e−2 | 25e−4 | 25e−6 |
| $\|e_{\omega_b}\|_{L^\infty}$ | 66e−1 | 51e−3 | 65e−5 | – | 28e2 | 21e0 | – | 26e0 | 25e−2 | – | 26e0 | 25e−2 |

Table 1: Performance measures for controllers (9), (17) ($\|u_a\|_{L^2}$, $\|e_{R_a}\|_{L^\infty}$, $\|e_{\omega_a}\|_{L^\infty}$) and (58) ($\|u_b\|_{L^2}$ ,$\|e_{R_b}\|_{L^\infty}$, $\|e_{\omega_b}\|_{L^\infty}$) at different sampling frequencies and for different values of gains. The performance achieved with (9),(17) is robust to variations on the gain values maintaining both, energy and precision, with almost no change.

For the simulation of the closed-loop, we consider two sampling times, denoted as $h_p$ and $h_c$, so that $h_p << h_c$. The sampling time $h_p = 50\mu s$ is used for integrating the kinematic and dynamic equations in (44), simulating a continuous time process in a digital computer, whereas $h_c$ is used for updating the values of the controller $\tau_k$. Thereby, the hybrid setup depicted in Figure 1 is approximated. We consider three cases for the updating time of the controller. Concretely, *i*) $h_c = 333ms$, *ii*) $h_c = 33ms$, and *iii*) $h_c = 3ms$. Regarding the parameters of the plant, we take $J = \mathrm{diag}(3, 4, 5)$ with initial conditions

$$R_0 = \begin{bmatrix} 0.6862 & 0.1905 & 0.7019 \\ 0.7261 & -0.2363 & -0.6456 \\ 0.0428 & 0.9527 & -0.3005 \end{bmatrix}, \text{ and } \omega_0 = 0\,.$$

For the disturbance we consider the signal

$$d(t) = \begin{bmatrix} \sin(5t)\cos(\sqrt{3}t) \\ \cos(\frac{\pi}{2}t)^2 \\ 2\cos(2t)\sin(\frac{t}{2})e^{-2\sin(t)} \end{bmatrix}, \tag{57}$$

with the upper-bound $\eta = 24$ in all simulations, whereas the parameters of the controller (9),(17) are set to $\kappa = 1$, $\gamma_1 = 15$, $\gamma_2 = 30$, and $\alpha_1 = \alpha_2 = 0$. For comparison purposes, we also consider the forward-Euler discretization of the multivariable super-twisting controller proposed in [35], that is

$$u_k = \nu_k - \gamma_1 \frac{z_{1,k}}{\|z_{1,k}\|_2^{\frac{1}{2}}}\,, \tag{58a}$$

$$\nu_{k+1} = \nu_k - h\gamma_2 \frac{z_{1,k}}{\|z_{1,k}\|_2}\,, \tag{58b}$$

with the same values of gains $\gamma_1$ and $\gamma_2$ as for the proposed controller. The time trajectories of the error signals $e_R(t) = \|I - R(t)\|_2$ and $e_\omega(t) = \|\omega(t)\|_2$ are plotted in Figure 2, whereas Figure 3 displays the associated control inputs. It is shown that, with the selected gains, the unitary super-twisting controller of Proposition 4 achieves a superior performance for low frequency sampling, when compared to the explicit discretization (58), whereas both controllers become alike for high frequencies. Also notice that the forward controller (58) shows a chattering level higher than that of (9),(17).

In order to compare the performance of both controllers, we consider the $L^2$-norm of the control input and the $L^\infty$-norm of its associated error signals once the ultimate bound is reached [2]. The former performance index quantifies the energy expended by the controller, whereas the latter quantifies the precision achieved. Table 1 shows the obtained performance measures for sampling frequencies in the set $\{3, 30, 300\}$ (samples per second) and for four cases *a*) $\gamma_1 = 15, \gamma_2 = 30$; *b*) $\gamma_1 = 0.1, \gamma_2 = 300$; *c*) $\gamma_1 = 300, \gamma_2 = 24$; and *d*) $\gamma_1 = 300, \gamma_2 = 300$. Once more, the proposed controller shows a remarkable performance even at low frequencies. Note that the controller (9),(17) has a strong insensitivity to changes on the gains, as it shows no change on precision, as predicted by Corollary 8. On the contrary, the controller (58) shows an important degradation of performance to the same change. Such invariance of performance with respect large gains for (9),(17) is due to the fact that the controller is the result of a *selection process*. This is reminiscent of first-order set-valued sliding-mode controllers, see *e.g.*, [20, 31]. This robustness property and the improved performance, with respect to (58), become important in applications with limited resources, such as satellite attitude control in spatial applications. ⌟

## 6 Approximation of the control law via proximal splitting algorithms

The explicit structure of the proposed super-twisting-like algorithm (10) always involves the proximal map of the sum of at least two convex functions, (*cf.*, (16)). In general, such proximal maps are difficult to compute. In such situations, proximal splitting algorithms [10, 39] become a central tool, providing a sequence that approximates the controller and that involves the proximal maps of simpler functions. In this section we study the implementation of the controller via a modified version of the celebrated Douglas-Rachford splitting [29, 13]. Let us consider the following control strategy in the style of (9)

$$u_{c,k} = -K(\gamma_1 m_{1,k} + h\gamma_2 m_{2,k}) + \nu_{k+1} \tag{59a}$$

$$\nu_{k+1} = \nu_k - h\gamma_2 K m_{2,k} \tag{59b}$$

$$m_{1,k} \in \partial f_1\left(\varrho(x_k, u_k) + h^2\gamma_2(m_{2,k} - m_{2,k-1})\right) \tag{59c}$$

$$m_{2,k} \in \partial f_2(\varrho(x_k, u_k)) \tag{59d}$$

[2] With the range of sampling frequencies studied here, the ultimate bound is reached after $t > 15s$.

As before, we take $z_{1,k} = K^{-\frac{1}{2}} x_k$, $z_{2,k} = K^{-\frac{1}{2}}(\nu_{k+1} + \bar{d}_k)$, $\hat{m}_{i,k} = K^{\frac{1}{2}} m_{i,k}$, $\hat{f}_i = f_i \circ K^{\frac{1}{2}}$, $i \in \{1,2\}$, and $\tilde{z}_{1,k+1} = \varrho(x_k, u_k) = z_{1,k} - h(\gamma_1 \hat{m}_{1,k} + h\gamma_2 \hat{m}_{2,k})$, so that the closed-loop (8), (59) becomes

$$z_{1,k+1} = \tilde{z}_{1,k+1} + h z_{2,k+1} \tag{60a}$$
$$z_{2,k+1} = z_{2,k} - h\gamma_2 \hat{m}_{2,k} + h\hat{\Delta}_{k-1} \tag{60b}$$
$$\tilde{z}_{1,k+1} = z_{1,k} - h(\gamma_1 \hat{m}_{1,k} + h\gamma_2 \hat{m}_{2,k}) \tag{60c}$$
$$\hat{m}_{1,k} \in \partial \hat{f}_1 \left( \tilde{z}_{1,k+1} + h^2 \gamma_2 (\hat{m}_{2,k} - \hat{m}_{2,k-1}) \right) \tag{60d}$$
$$\hat{m}_{2,k} \in \partial \hat{f}_2 (\tilde{z}_{1,k+1}) \tag{60e}$$

**Proposition 10.** *The closed-loop* (60) *is well-posed and the selection of values* $\hat{m}_{1,k}$ *and* $\hat{m}_{2,k}$ *is given by*

$$\hat{m}_{1,k} = \frac{1}{h\gamma_1} \left( \mathrm{Id} - \mathrm{Prox}_{h\gamma_1 \hat{f}_1} \right) \left( z_{1,k} - \left( \mathrm{Id} - \mathrm{Prox}_{h^2\gamma_2 \hat{f}_2} \right) (\vartheta_k) \right) , \tag{61a}$$
$$\hat{m}_{2,k} = \frac{1}{h^2\gamma_2} (\mathrm{Id} - \mathrm{Prox}_{h^2\gamma_2 \hat{f}_2})(\vartheta_{k+1}) , \tag{61b}$$

*where* $\vartheta_k$ *satisfies the recursive equation*

$$\vartheta_{k+1} = \mathrm{Prox}_{h\gamma_1 \hat{f}_1} \left( z_{1,k} - \left( \mathrm{Id} - \mathrm{Prox}_{h^2\gamma_2 \hat{f}_2} \right) (\vartheta_k) \right) + \left( \mathrm{Id} - \mathrm{Prox}_{h^2\gamma_2 \hat{f}_2} \right) (\vartheta_k) , \tag{62}$$

*where* $\vartheta_0 \in \mathbb{R}^n$ *is arbitrary.*

*Proof.* Let $\vartheta_{k+1} = \tilde{z}_{1,k+1} + h^2\gamma_2 \hat{m}_{2,k}$. Thus, from (60e) it follows that

$$\tilde{z}_{1,k+1} = \mathrm{Prox}_{h^2\gamma_2 \hat{f}_2}(\vartheta_{k+1}) , \tag{63}$$

and consequently $\hat{m}_{2,k}$ satisfies (61b). On the other hand, let $\xi_{k+1} = \tilde{z}_{1,k+1} + h^2\gamma_2(\hat{m}_{2,k} - \hat{m}_{2,k-1})$. From (60c), together with (61b), we obtain that

$$\xi_{k+1} + h\gamma_1 \hat{m}_{1,k} = z_{1,k} - (\mathrm{Id} - \mathrm{Prox}_{h^2\gamma_2 \hat{f}_2})(\vartheta_k) \tag{64}$$

and (60d) leads us to

$$\xi_{k+1} = \mathrm{Prox}_{h\gamma_1 \hat{f}_1} \left( z_{1,k} - (\mathrm{Id} - \mathrm{Prox}_{h^2\gamma_2}\, \hat{f}_2)(\vartheta_k) \right) . \tag{65}$$

Now, from (64) and (65) the expression for $\hat{m}_{1,k}$ in (61a) is obtained. In addition, from the definitions of $\vartheta_{k+1}$ and $\xi_{k+1}$ we have that

$$\vartheta_{k+1} = \tilde{z}_{1,k+1} + h^2\gamma_2 \hat{m}_{2,k} = \xi_{k+1} + h^2\gamma_2 \hat{m}_{2,k-1} , \tag{66}$$

so that (62) follows from (61b) and (65). The well-posedness of the closed-loop (60) is immediate, as all the variables depend on known quantities at time $t_k = kh$. This concludes the proof. □

**Remark 1.** *The scheme* (60c)-(60e) *is reminiscent of the famous Douglas-Rachford splitting applied to the generalized equation*

$$z_2 \in \gamma_1 \partial \hat{f}_1(z_1) + h\gamma_2 \partial \hat{f}_2(z_1) . \tag{67}$$

*Indeed, it follows from* (60a) *and from* (63) *that*

$$z_{1,k} = \mathrm{Prox}_{h^2\gamma_2 \hat{f}_2}(\vartheta_k) + h z_{2,k} .$$

*Thus,* (62) *becomes*

$$\vartheta_{k+1} = \mathrm{Prox}_{h\gamma_1 \hat{f}_1} \left( 2\,\mathrm{Prox}_{h^2\gamma_2 \hat{f}_2}(\vartheta_k) - \vartheta_k + h z_{2,k} \right) + (\mathrm{Id} - \mathrm{Prox}_{h^2\gamma_2 \hat{f}_2})(\vartheta_k) , \tag{68}$$

*which is the classical Douglas-Rachford splitting associated with* (67)*, see [10, 13, 29] for further details and properties about the Douglas-Rachford splitting.* ⌟

**Corollary 11.** *Consider the closed-loop* (60) *and let all assumptions of Theorem 7 hold. Let* $\partial \hat{f}_1$ *be locally bounded and let* $\partial \hat{f}_2$ *be uniformly bounded. Then, there exist* $h > 0$ *sufficiently small and gains* $\gamma_1 > 0$, $\gamma_2 > \eta$ *sufficiently large, such that* $\tilde{z}_{1,k+1}$ *reaches the origin after a finite-number of steps.* ⌟

*Proof.* The proof follows the same steps as the proof of Theorem 7 together with the use of the outer semicontinuity of $\partial\hat{f}_1$. Indeed, as $\hat{m}_{2,k}$ is uniformly bounded by assumption, then $\tilde{z}_{1,k+1} + h^2\gamma_2(\hat{m}_{2,k} - \hat{m}_{2,k-1})$ is in a $\mathcal{O}(h^2)$ neighborhood of $\tilde{z}_{1,k+1}$. It follows from (60d) that, for any $\varepsilon > 0$, there is $h > 0$ sufficiently small such that $\hat{m}_{1,k} \in \partial\hat{f}_1(\tilde{z}_{1,k+1}) + \varepsilon\mathcal{B}$ [8, Proposition 2.5.24-i)]. Thus, as $\partial\hat{f}_1$ is a $\theta$-monotone map, it follows that

$$\langle \hat{m}_{1,k} - \hat{m}_{1,k-1}, \tilde{z}_{1,k+1} - \tilde{z}_{1,k} \rangle \geq (\theta(\tilde{z}_{1,k+1}, \tilde{z}_{1,k}) - \varepsilon)\|\tilde{z}_{1,k+1} - \tilde{z}_{1,k}\| \,. \tag{69}$$

The rest of the proof follows as the proof of Theorem 7 *mutatis mutandis.* □

**Example 12.** *Let us consider once more the attitude stabilization problem described in Section 5. For the controller, let us take this time* (59) *with* $f_1(\cdot) = \frac{2}{3}\|\cdot\|_1^{\frac{3}{2}}$, $f_2(\cdot) = \|\cdot\|_2$. *Notice that, in this case, an explicit expression for the proximal map* $\mathrm{Prox}_{hg}$, *with* $g = \gamma_1\hat{f}_1 + h\gamma_2\hat{f}_2$, *is hard to obtain. Nevertheless, the proposed Douglas-Rachford-based splitting allows us to compute an approximation in an iterative way. Following a procedure similar to the one presented in Proposition 4, the proximal maps to* $h\gamma_1\hat{f}_1$ *and* $h^2\gamma_2\hat{f}_2$ *are computed as*

$$[\mathrm{Prox}_{h\gamma_1\hat{f}_1}(p)]_i = \begin{cases} 0, & \text{if } |p_i| \leq h\gamma_1\kappa^{\frac{3}{4}}\tilde{q}(\|p\|_1)\,; \\ p_i - h\gamma_1\kappa^{\frac{3}{4}}\tilde{q}(\|p\|_1)\,\mathrm{sgn}(p_i), & \text{otherwise}\,. \end{cases} \tag{70a}$$

$$\mathrm{Prox}_{h^2\gamma_2\hat{f}_2}(p) = \begin{cases} 0, & \text{if } \|p\|_2 \leq h^2\gamma_2\kappa^{\frac{1}{2}}\,; \\ p - \frac{h^2\gamma_2\kappa^{\frac{1}{2}}}{\|p\|_2}p, & \text{otherwise}\,. \end{cases} \tag{70b}$$

*where,* $p \in \mathbb{R}^n$ *and*

$$\tilde{q}(v) = \frac{-h\gamma_1\kappa^{\frac{3}{4}}n + \sqrt{(h\gamma_1\kappa^{\frac{3}{4}}n)^2 + 4v}}{2}\,. \tag{71}$$

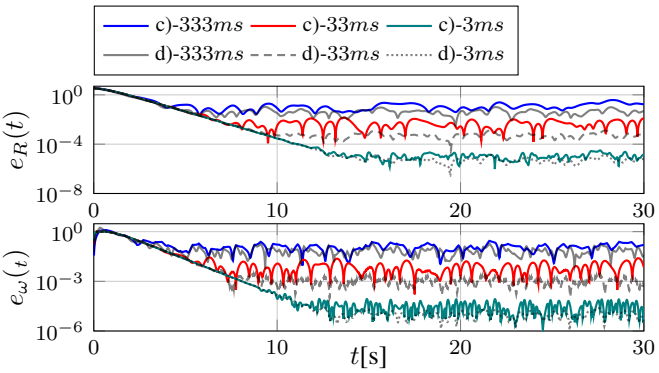


Figure 4: Time trajectories of the error norms $e_R(t) = \|I - R(t)\|_2$ and $e_\omega(t) = \|\omega(t)\|_2$ for three different sampling times ($333ms, 33ms$, and $3ms$). Case c) corresponds to trajectories with the feedback (59), whereas case d) corresponds to trajectories with the feedback (72)-(73). In all cases the system is affected by the disturbance (57).

*As a comparison, we also consider the calculation of the controller* (9) *by using the numerical solver CLARABEL [1]. That is, at each sampling interval, we solve the optimization problem*

$$\mathrm{Prox}_{hg}(z_{1,k}) = \underset{w\in\mathbb{R}^n}{\arg\min}\left\{\gamma_1\hat{f}_1(w) + h\gamma_2\hat{f}_2(w) \quad + \frac{1}{2h}\|w - z_{1,k}\|_2^2\right\}. \tag{72}$$

*So that, with the help of* (15) *and* (16), *the controller* (9) *becomes*

$$u_{d,k} = \nu_{k+1} - \frac{\kappa^{\frac{1}{2}}}{h}\left(\mathrm{Id} - \mathrm{Prox}_{hg}\right)(z_{1,k}), \tag{73a}$$

$$\nu_{k+1} = \begin{cases} \nu_k - \frac{\kappa^{\frac{1}{2}}}{h}z_{1,k}, & \text{if } \|\mathrm{Prox}_{hg}(z_{1,k})\| \leq 1\times 10^{-9}\,; \\ \nu_k - \frac{h\gamma_2\kappa^{\frac{1}{2}}}{\|\mathrm{Prox}_{hg}(z_{1,k})\|_2}\mathrm{Prox}_{hg}(z_{1,k}), & \text{otherwise}\,. \end{cases} \tag{73b}$$

*Setting $\kappa = 1$, $\gamma_1 = 15$ and $\gamma_2 = 30$, Figure 4 shows the resulting closed-loop error trajectories for the system with feedback (59) and (73), whereas Figure 5 displays the associated control inputs. Even though the errors are very similar, it is worth to mention that the calculation of (72)-(73) takes between $1.9ms$ to $2.0ms$ at each iteration, whereas the calculation of (59), via (61) and (70)-(71), takes between $165\mu s$ to $200\mu s$ at each iteration. So that the proposed splitting is approximately 10 times faster than the numeric approach (72)-(73). In any case, both approaches are entirely feasible with the range of sampling frequencies considered here. As a final remark, in this example (and the previous one), all the simulations were coded in Python 3 and all of them were performed on an standard laptop (8 GB of RAM memory, 4-cores CPU running at 2.8GHz).* ⌟

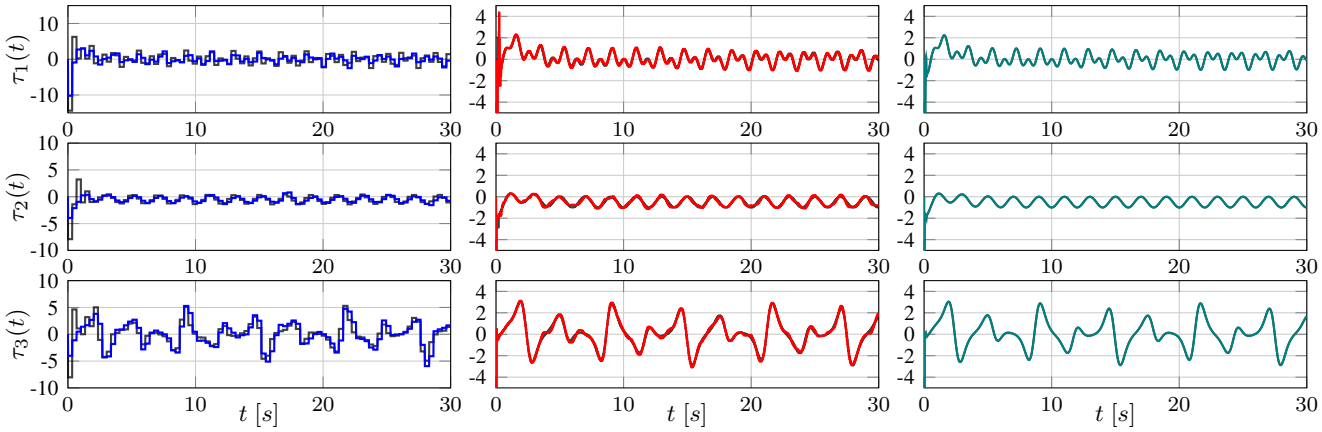


Figure 5: Time evolution of the control input $\tau(t) = \tau_k$ for $t \in [kh, (k+1)h)$ with $\tau_k$ as in (55) for three different sampling times ($333ms$ (left column), $33ms$ (central column) and $3ms$ (right column)). For each sampling time, two cases are considered. *i)* $u_k$ as in (59) (color lines) and *ii)* $u_k$ as in (72)-(73) (gray lines).

## 7 Conclusions

A family of discrete-time super-twisting-like algorithms for control was introduced and its well-posedness, as well as, its stability and robustness properties were analyzed. Contrary to most of the literature on super-twisting algorithms, the presented theoretical analysis makes no use of homogeneity properties of the vector field, but instead it is based on the maximal monotonicity of the maps defining the controller. This approach opens an alternative way for studying higher order sliding-mode controllers based on variational methods. Moreover, an adaptation of the Douglas-Rachford splitting, for the implementation of the control law, was also studied. Numerical simulations illustrate how the proposed family of controllers surpass the performance of conventional forward-Euler emulation-based designs.

## References


[1] CLARABEL solver. htpps://oxfordcontrol.github.io/ClarabelDocs/stable/. Accessed: 18-03-2024.

[2] V. Acary, B. Brogliato, and Y. V. Orlov. Chattering-free digital sliding-mode control with state observer and disturbance rejection. *Automatic Control, IEEE Transactions on*, 57(5):1087–1101, 2012.

[3] B. Andritsch, L. Watermann, S. Koch, M. Reichhartinger, J. Reger, and M. Horn. Modified implicit discretization of the super-twisting controller. *IEEE Transactions on Automatic Control*, 2024. https://doi.org/10.1109/TAC.2024.3370494.

[4] I. Balogoun, S. Marx, T. Liard, and F. Plestan. Super-twisting sliding mode control for the stabilization of a linear hyperbolic system. *IEEE Control System Letters*, 7:1–6, 2023.

[5] M. Basin, C. B. Panathula, and Y. Shtessel. Multivariable continuous fixed-time second-order sliding mode control: design and convergence time estimation. *IET Control & Applications*, 11(8):1104–1111, 2017.

[6] H. H. Bauschke and P. L. Combettes. *Convex Analysis and Monotone Operator Theory in Hilbert Spaces*. CMS Books in Mathematics. Springer New York, 2011.

[7] B. Brogliato, A. Polyakov, and D. Efimov. The implicit discretization of the super-twisting sliding-mode control algorithm. *IEEE Transactions on Automatic Control*, 65(8):3707–3713, 2020.

[8] R. S. Burachik and A. N. Iusem. *Set-valued Mappings and Enlargements of Monotone Operators*. Springer, New York, USA, 2008.

[9] N. A. Chaturdevi, A. K. Sanyal, and N. H. McClamroch. Rigid-body attitude control: using rotation matrices for continuous singularity-free control laws. *IEEE Control Systems Magazine*, 31(3):30–51, 2011.

[10] L. Condat, D. Kitahara, A. Contreras, and A. Hirabayashi. Proximal splitting algorithms for convex optimization: a tour of recent advances, with new twists. *SIAM Review*, 65(2), 2023.

[11] L. Dávila, J. Fridman and A. Levant. Second-order sliding-mode observer for mechanical systems. *IEEE Transactions on Automatic Control*, 50(11):1785–789, 2005.

[12] L. Derafa, A. Benallegue, and L. Fridman. Super twisting control algorithm for the attitude tracking of a four rotors uav. *Journal of the Franklin Institute*, 349:685–699, 2012.

[13] J. Eckstein and D. P. Bertsekas. On the Douglas-Rachford splitting method and the proximal point algorithm for maximal monotone operators. *Mathematical Programming*, 55:293–318, 1992.

[14] C. Evangelista, P. Puleston, F. Valenciaga, and L. M. Fridman. Lyapunov-designed super-twisting sliding mode control for wind energy conversion optimization. *IEEE Transactions on Industrial Electronics*, 60(2):538–545, 2013.

[15] T. Floquet and J. P. Barbot. Super twisting algorithm-based step-by-step sliding mode observers for nonlinear systems with unknown inputs. *International Journal of Systems Science*, 38(10):803–815, 2007.

[16] G. F. Franklin, J. D. Powell, and M. L. Workman. *Digital Control of Dynamical Systems*. Ellis-Kagle Press, CA, USA, third edition, 2006.

[17] R. Goebel, R. G. Sanfelice, and A. R. Teel. *Hybrid Dynamical Systems: Modeling, Stabilitym and Robustness*. Princenton University Press, New Jersey, USA, third edition, 2012.

[18] G. C. Gómez Cortés, F. Castaños, and J. Dávila. Sliding motions on $SO(3)$, sliding subgroups. In *Decision and Control, 2019 58th IEEE Conference on*, pages 6953–6958, Nice, France, Dec.

[19] A. Hanan, A. Jbara, and A. Levant. Low-chattering discretization of sliding modes. In T. R. Oliveira, L. Fridman, and L. Hsu, editors, *Sliding-mode Control and Variable-Structure Systems*, Studies in Systems, Decision and Control, pages 229–264. Springer, 2023.

[20] O. Huber, V. Acary, and B. Brogliato. Lyapunov stability and performance analysis of the implicit discrete sliding mode control. *IEEE Transactions on Automatic Control*, 61(10):3016–3030, 2016.

[21] O. Huber, B. Brogliato, V. Acary, A. Boubakir, F. Plestan, and B. Wang. Experimental results on implicit and explicit time–discretization of equivalent–control–based sliding mode control. In L. Fridman, J.-P. Barbot, and F. Plestan, editors, *Recent Trends in Sliding Mode Control*, pages 207–236. The IET, 2016.

[22] P. Kaveh and Y. B. Shtessel. Blood glucose regulation using high-order sliding mode control. *International Journal of Robust and Nonlinear Control*, 18:557–569, 2008.

[23] S. Koch and M. Reichhartinger. Discrete-time equivalents of the super-twisting algorithm. *Automatica*, 107:190–199, 2019.

[24] V. Lakshmikantham and D. Trigiante. *Theory of Difference Equations: Numerical Methods and Applications*. Academic Press Inc., San Diego, CA, USA, 1988.

[25] S. László. $\theta$-monotone operators and $\theta$-convex functions. *Taiwanese Journal of Mathematics*, 16(2):733–759, 2012.

[26] A. Levant. Sliding order and sliding accuracy in sliding mode control. *International Journal of Control*, 58(6):1247–1263, 1993.

[27] A. Levant. Robust exact differentiation via sliding mode technique. *Automatica*, 34(3):379–384, 1998.

[28] D. Liberzon. *Switching in Systems and Control*. Birkhäuser, New York, USA, 2003.

[29] P. L. Lions and B. Mercier. Splitting algorithms for the sum of two nonlinear operators. *SIAM Journal on Numerical Analysis*, 16(6):964–979, 1979.

[30] F. López-Caamal and J. A. Moreno. Generalised mutivariable supertwisting algorithm. *International Journal of Robust and Nonlinear Control*, 29:634–660, 2019.

[31] F. Miranda-Villatoro, B. Brogliato, and F. Castaños. Set-valued sliding-mode control of uncertain linear systems: continuous and discrete-time analysis. *SIAM Journal on Control and Optimization*, 56(3):1756–1793, 2018.

[32] R. Mojallizadeh, B. Brogliato, A. Polyakov, S. Selvarajan, L. Michel, F. Plestan, M. Ghanes, J.-P. Barbot, and Y. Aoustin. A survey on the discrete-time differentiators in closed-loop control systems: experiments on an electro-pneumatic system. *Control Engineering Practice*, 136:105546, 2023.

[33] J. A. Moreno and M. Osorio. Strict Lyapunov functions for the super-twisting algorithm. *IEEE Transactions on Automatic Control*, 57(4):1035–1040, 2012.

[34] J. A. Moreno, H. Ríos, L. Ovalle, and L. Fridman. Multivariable super-twisting algorithm for systems with uncertain input matrix and perturbations. *IEEE Transactions on Automatic Control*, 67(12):6716–6722, 2022.

[35] I. Nagesh and C. Edwards. A multivariable super-twisting sliding mode approach. *Automatica*, 50(3):984–988, 2014.

[36] A. Polyakov and A. Poznyak. Reaching time estimation for "super-twisting" second order sliding mode controller via Lyapunov function designing. *IEEE Transactions on Automatic Control*, 54(8):1951–1955, 2009.

[37] A. Poznyak. Stochastic super-twist sliding mode controller. *IEEE Transactions on Automatic Control*, 63(5):1538–1544, 2018.

[38] P. Prasun, S. Pandey, S. Kamal, S. Ghosh, and X. Xiong. A minimum operator based discrete-time super-twisting like algorithm. *IEEE Transactions on Circuits and Systems II: Express Briefs*, 71(1):286–290, 2023.

[39] E. K. Ryu and W. Yin. *Large-Scale Convex Optimization via Monotone Operators*. Cambridge University Press, New York, USA, 2023.

[40] Y. Shtessel, C. Edwards, L. Fridman, and A. Levant. *Sliding Mode Control and Observation*. Birkhäuser, 2014.

[41] V.I. Utkin. *Sliding Modes in Control and Optimization*. Communications and Control Engineering. Springer-Verlag, 1992.

[42] P. V. N. M. Vidal, E. V. L. Nunes, and L. Hsu. Output-feedback multivariable global variable gain super-twisting algorithm. *IEEE Transactions on Automatic Control*, 62(6):2999–3005, 2022.

[43] X. Xiong, G. Chen, Y. Lou, R. Huang, and S. Kamal. Discrete-time implementation of super-twisting control with semi-implicit Euler method. *IEEE Transactions on Circuits and Systems II: Express Briefs*, 69(1):99–103, 2022.

[44] K. Zhang, T. Hatano, T. T. Nguyen, C. Edwards, G. Herrmann, G. Burgess, M. Antognozzi, S. Khan, R. Harniman, and M. Miles. A super-twisting observer for atomic-force reconstruction in a probe microscope. *Control Engineering Practice*, 94:104191, 2020.